Original Article

An *ex vivo* study of auranofin efficacy in the treatment of cryptosporidiosis

Esraa G El-saadi[1], Fetouh A Deyab[1], Howaida IH Ismail[1], Mona T Sadek[2], Heba H Elkaliny[2], Dina I Elgendy[1]

Departments of Medical Parasitology[1], and Histology[2], Faculty of Medicine, Tanta University, Egypt.

ABSTRACT

Background: Because Nitazoxanide (NTZ) shows limited efficacy in immunosuppressed individuals, a search for a safe and more effective alternative is urgently required. Auranofin (AUR) showed potent anti-inflammatory and anti-parasitic effects against numerous helminthic and protozoan parasites.
Objective: To evaluate the *ex vivo* effects of AUR on *C. parvum* in comparison with NTZ.
Material and Methods: Collected ileal explants were inoculated with excysted *C. parvum* oocysts in a dose of 10^4 oocysts/well. Six-well culture plates were used to grow 5 groups of ileal explants designated as two control groups (uninfected, and infected), and three treated groups (NTZ, AUR, and both drugs). The drugs were added six hours post-infection (PI). After 24 h of the drug treatment, explants from all groups were collected and processed for histopathological and ultrastructural assessments, and the culture supernatants were used for assessment of IFN-γ, IL-1β, IL-10, and thioredoxin reductase (TrxR) levels.
Results: Compared to infected control group, histopathological and ultrastructural examination revealed significant (P<0.001) restoration of the normal intestinal structure in the combined-treated group, followed by the AUR-treated group, while the NTZ group exhibited only partial improvement with persistent pathological changes in enterocytes, and marked ultrastructural abnormalities. Both NTZ and AUR showed significant (P<0.001) reduction in IFN-γ and IL-1β levels and a significant (P<0.001) increase in IL-10 levels. The addition of NTZ induced an insignificant elevation in TrxR levels in intestinal tissue compared to the infected control group. The lowest level of TrxR enzyme was recorded in the AUR group.
Conclusion: Our study concluded that AUR demonstrated superior anti-cryptosporidial, and anti-inflammatory efficacy compared to NTZ, likely due to its redox-modulating activity. The combination group showed the best results. Further *in vivo* studies, and human clinical trials are recommended.

Keywords: auranofin; cryptosporidiosis; electron microscopy; *ex vivo*; IFN-γ; IL-1β; IL-10; nitazoxanide; thioredoxin reductase.

Received: 26 July, 2025; **Accepted:** 20 August, 2025.

Corresponding Author: Dina I. Elgendy; **Tel.:** +20 1063756432; **Email:** dina.elgendy@med.tanta.edu.eg

Print ISSN: 1687-7942, **Online ISSN:** 2090-2646, **Vol. 18, No. 2, August, 2025.**

INTRODUCTION

Cryptosporidium spp. are obligate intracellular protozoan parasites belonging to the phylum Apicomplexa. Currently, there are 47 species and more than 100 genotypes of *Cryptosporidium* that affect vertebrate hosts, of which the zoonotic *C. parvum* and the anthroponotic *C. hominis* are the primary causes of human cryptosporidiosis worldwide[1]. They are responsible for numerous waterborne outbreaks, as well as life-threatening opportunistic infections in patients with AIDS. *Cryptosporidium* is also one of the top four diarrhea-causing agents that affect children in developing countries[2]. Furthermore, significant morbidity and mortality due to cryptosporidiosis occur mainly in children[3].

There are currently limited treatment options for cryptosporidiosis, and NTZ is the only medication, approved by the Food and Drug Administration (FDA) for its treatment[4]. However, NTZ has shown limited efficacy in immunocompromised patients, particularly HIV-infected children, and it is not FDA-approved for these patients. Additionally, resistance to NTZ has been demonstrated[5]. Hence, it is critical to search for alternative and more effective drugs for treating cryptosporidiosis.

Auranofin, an FDA-approved drug containing gold, is used to treat rheumatoid arthritis[6]. It attracted researchers' attention as a potential alternative therapeutic agent for several illnesses, including AIDS, cancer, inflammation, and neurological diseases[7]. Additionally, it demonstrated efficacy against some parasitic, viral, and bacterial illnesses[8]. The efficacy of AUR was documented in inhibiting the viability, and development of numerous protozoan parasites, such as *T. vaginalis*[9], *Blastocystis* spp.[10], *N. fowleri*[11], as well as *L. tropica, T. gondii,* and *T. cruzi*[12]. Furthermore, it showed promising effects against helminthic infections, including adult filarial worms[13], and *S. mansoni*[14].

 DOI: 10.21608/puj.2025.407692.1310

The TrxRs are essential antioxidant enzymes found in bacteria, fungi, and some protozoan parasites, including apicomplexan parasites. These enzymes regulate intracellular reactive oxygen species (ROS) levels and help parasites withstand oxidative stress from their metabolism and the host immune response. Hence, they are essential for maintaining intracellular levels of ROS that provide resistance against internal and external oxidative stresses[15]. That's why they are considered potential therapeutic targets[6]. Studies on the therapeutic effects of auranofin showed its inhibitory effect on TrxR enzyme[8,16]. Furthermore, it has potent anti-inflammatory, and anti-fibrotic effects[17]. Thus, AUR has the potential to become an alternative therapeutic agent for cryptosporidiosis, and there is a need to evaluate its efficacy against *C. parvum*.

Ex vivo cultivation of *Cryptosporidium* is a method that can provide deeper insights into the parasite's pathophysiology and offer researchers more precise tools to assess new drugs[18]. The *in vitro* culture uses different types of cells, especially tumor cells. This technique fills the gap between *in vivo* research (performed within a living host) and *in vitro* research (performed by means of isolated cells in artificial environments). Compared to *in vivo* studies, *ex vivo* studies allow for more experimental control, preserving the tissue's natural structure and some biological function[19]. The *ex vivo* cultivation was preferred in the current study, aiming to assess the effectiveness of AUR on cryptosporidiosis. Hence, the use of the primary site of the infection, which is the intestine with its different cells (including epithelial, stromal, and resident leukocytes), was done to simulate the normal *in vivo* environment and help study the disease and drug effect.

MATERIAL AND METHODS

This randomized control experimental study was conducted in the Medical Parasitology Department, Faculty of Medicine, Tanta University, during the period from January 2023 to July 2025.

Study design: The current study was designed to assess the efficacy of AUR against *C. parvum*. For this aim collection of buffalo ileal tissues and *ex vivo* cultivation were done. The drugs were added six hours PI. After 24 h of drug treatment, the explants from all groups were collected and handled for examination using light and electron microscopy. The culture media were collected for assessment of cytokines (IFN-γ, IL-1β, and IL-10) and TrxR levels.

Collection of buffalo ileal tissues: Buffalo ileal tissues were obtained from a local slaughterhouse in Tanta, and immediately preserved in cold sterile saline solution supplemented with 50 µg/ml of 1% gentamicin (Alex Co., Egypt) to prevent microbial contamination. The samples were rapidly transferred to the culture laboratory. Samples were washed once with 70% alcohol to ensure surface decontamination, and then washed five times with warm sterile saline solution (NaCl 0.9%) to remove any residual disinfectant and debris, ensuring the samples were adequately clean for preparation of tissue explants prior to *ex vivo* cultivation.

Preparation of tissue explants: They were prepared as described by Aboelsoued *et al.*[20]. Briefly, the ileal segments were divided with a sterile scalpel into small pieces (40–60 mg each), then randomly placed, with the mucosa facing upwards, into 5 six-well culture plates, one piece per well containing 1.5 ml of Roswell Park Memorial Institute medium (RPMI-1640), L-glutamine, 50 µg/ml of 1% gentamicin and 10% fetal bovine serum (FBS). The culture plates were then incubated at 37°C and 5% CO_2 in a humidified CO_2 incubator for 2 h to allow tissue stabilization. Subsequently, the ileal explants were relocated to new culture plates, and new, freshly prepared media were then added as previously described. All procedures were performed under aseptic conditions within a Class II laminar flow biosafety cabinet to prevent microbial contamination.

The parasite: The Biological Supply Program at the Theodor Bilharz Research Institute (BSP/TBRI), Imbaba, Giza, Egypt, provided the *C. parvum* oocysts. The providing institute had previously genotyped and documented the parasite.

***Cryptosporidium* oocyst excystation for infection of the tissue explants:** Excystation was performed as previously described[20]. Liberation of sporozoites was achieved by pre-treating *C. parvum* oocysts with acidified (pH 2.0) and pre-warmed (37°C) 1× Hank's Balanced Salt Solution (HBSS), calcium- and magnesium-free (Biowest, France), for 10 min at 37°C. The solution was then centrifuged at 4000×g at 4 °C for 3 min. The pellet was incubated in pre-warmed (37°C), non-acidified 1× HBSS for another 10 min at 37°C. After discarding the supernatant, the pellet was resuspended in excystation medium containing pre-warmed (37°C) RPMI-1640 with L-glutamine and 10% FBS for 30 min. The suspension was transferred to 2 ml microcentrifuge tubes and centrifuged again at 4000×g at 4 °C for 3 min. Finally, the excystation medium was immediately added to the tissue explants in the wells at a dose of 10^4 excysted oocysts/well for induction of infection.

Drugs: The control drug (NTZ) was obtained from Medizen Pharmaceutical Industries for Utopia Pharmaceuticals (Nanazoxid©, 100 mg/5 ml suspension). Ileal explants were treated with NTZ at a concentration of 10 µg/ml[21]. The required concentration was obtained by dilution with distilled water. The test drug (AUR, 10 mg powder) was obtained from Sigma-Aldrich, Cairo. It was dissolved

in 100% dimethyl sulfoxide (DMSO) to get a solution with a final concentration of 5 mg/ml. Dissolved AUR was further diluted in complete tissue culture medium (RPMI-1640) plus FBS for a final AUR concentration of 2 μM[22].

Study groups: The culture plates of the ileal explants were divided into 5 groups as follows: GI: uninfected (negative control); GII: infected, untreated (positive control); GIII: NTZ-treated infected explants; GIV: AUR-treated infected explants; GV: combined NTZ and AUR treatment

Histopathological study: According to Atallah *et al.*[23], the ileal explants were immediately fixed in neutral-buffered 10% formalin and stained with H & E. The ileal sections were then examined for microscopic detection of *Cryptosporidium* stages. The histopathological semiquantitative scoring to evaluate specific pathological changes was done as follows: inflammatory cellular infiltrate (<10%: minimal, 10-25%: mild, 26-50%: moderate, >50%: severe); interruption of the lining epithelium (<25%: minimal, 25-35%: mild, 36-50%: moderate, >50%: severe); separation of the lining cells from the underlying basement membrane (<25%: minimal, 25-35%: mild, 36-50%: moderate, >50%: severe). Five non-overlapping microscopic fields in each slide were examined using ×400 magnification.

Scanning electron microscopic (SEM) study[24]: The ileal specimens were initially fixed in 2.5% glutaraldehyde for 24 h, rinsed twice in phosphate-buffered saline (PBS) for 15 min each, and postfixed in 1% osmium tetroxide for two hours. The samples were subsequently rinsed twice with PBS for 15 min each, dehydrated in ascending grades of alcohol, and dried using a CO2 critical point drier (Audosamdri-815, Tousimis; Rockville, Maryland, USA). Finally, the specimens were mounted on aluminum stubs, gold-coated using a gold sputter coater (SPI- Module, USA), examined, and photographed with SEM (JSM- 5500 LV; JEOL Ltd- Japan) at the Electron Microscopic Unit, Faculty of Medicine, Tanta University.

Transmission electron microscopic (TEM) study[25]: The ileal specimens were divided with a sharp razor blade into 1 mm^3 pieces, then fixed in 2.5% glutaraldehyde for 2 h at 4°C, rinsed three times with PBS (10 min each), and postfixed in 1% osmium tetroxide for 30 min. The specimens were washed another three times in PBS, 30 min each, then dehydrated in ascending grades of alcohol. The specimens were then transferred into acetone, then into acetone and epoxy resin mixtures, and finally into pure epoxy resin. The next day, each sample was transferred individually to the tip of a labeled epoxy resin capsule, and an accelerator [2, 4, 6-tri-dimethylaminomethyl phenol-30 (DMP-30)] was added. The capsules were polymerized in an oven (60°C), then removed, cooled, trimmed, and sliced into 1 μm thick semithin sections using an ultramicrotome. The semithin sections were mounted on glass slides, stained with toluidine blue, and examined with a light microscope to choose suitable areas for ultrathin sectioning. Hence, the block face was re-trimmed using a diamond knife, and 75 nm thick ultrathin sections were cut using an ultramicrotome. These sections were picked on copper grids, then double-stained, first with uranyl acetate solution for 30 min, counter-stained with lead citrate for less than 10 min, finally washed with distilled water and dried on clean filter paper. The ultrathin sections were examined and photographed using (JEOL-JEM-100 SX electron microscope, Japan) at the Electron Microscopic Unit, Faculty of Medicine, Tanta University, Egypt.

Assessment of immunological and biochemical markers in the culture supernatants: Immunological and biochemical markers concentrations were assessed in the collected culture supernatants. The pro-inflammatory cytokines (IFN-γ, IL-1β), as well as the anti-inflammatory cytokine (IL-10), were measured using commercially available ELISA kits based on the Sandwich-ELISA principle. Specifically, IFN-γ Cytokine Assay ELISA Kit (Catalog No. MBS2500105), IL-1β Assay ELISA Kit (Catalog No. ELK1271), and IL-10 Assay ELISA Kit (Catalog No. MBS704754) were used, respectively. In addition, TrxR enzyme activity was evaluated using the Thioredoxin Reductase Assay ELISA kit (Catalog No. 201-02-0144) following the manufacturer's instructions.

Statistical analysis: Data were analyzed using SPSS 24, IBM, Armonk, NY, United States of America. Quantitative data were presented as mean±SD. Kruskal-Wallis test for abnormally distributed quantitative variables was used to compare more than two studied groups. Post Hoc test was used for multiple comparisons between different variables. Chi-square (X^2) test of significance was used in order to compare proportions between two qualitative parameters. Significance is considered when $P<0.05$.

Ethical consideration: The study was approved by the Ethics Committee of the Faculty of Medicine, Tanta University. The ethical approval number for this study is 36264MD11/1/23.

RESULTS

Histopathological results: Histological examination of the ileal explants revealed different pathological changes across the studied groups. GI (negative uninfected explant group) showed normal ileal epithelium that was formed of columnar enterocytes with intact brush border and oval basal nuclei, in addition to goblet cells with apical mucous granules (Fig. 1A). In contrast, GII (positive infected explant

group) showed severe interruption of the lining epithelium and separation of the lining cells from the underlying basement membrane, in addition to severe mononuclear cellular infiltration of the lamina propria. Multiple different developmental stages of *C. parvum* were detected adhering to the mucosal surface and at sites of the epithelial disruption (Fig. 1B). The previous changes were still reported in GIII (NTZ-treated infected explants), where multiple different-sized parasitic stages were seen along the ileal surface. Moderate to severe disruption of the epithelial lining and its separation from the underlying basement membrane, in addition to mononuclear cellular infiltration of the lamina propria, were also detected (Fig. 1C). The GIV (AUR-treated infected explants) showed few scattered oocysts spreading on the ileal surface with minimal to mild separation of the lining epithelium and mononuclear cellular infiltration of the lamina propria in some sections (Fig. 1D). Finally, GV (combined NTZ and AUR treatment) showed the least changes among all infected groups, where almost all sections revealed normal epithelium and intact brush border with occasional minimal focal disruption or separation of the lining epithelium in a few sections (Fig. 1E). These histopathological changes were compatible with the semiquantitative assessment scores summarized in table (1), further confirming the superior efficacy of combined NTZ and AUR treatment in alleviating *Cryptosporidium*-induced intestinal pathology.

Scanning electron microscopic results: SEM examination of the ileal explants obtained from GI (negative uninfected explant group) showed the normal architecture of the buffalo ileal mucosal surface. The enterocytes appeared polygonal with a dome-shaped upper surface and well-demarcated boundaries (Fig. 2A). Group II (positive infected explant group) showed a disturbed architecture of the ileal mucosal surface that appeared studded with numerous different-sized parasitic stages with regular, rounded shape and smooth surfaces. In addition, loss of the normal structure of the enterocytes was observed, where they appeared flattened with a rough surface and lost intercellular demarcations. Interruption of the mucosal surface with exposure of the underlying connective tissue of the lamina propria was also observed in some sections (Figs. 2B, 2C). Group

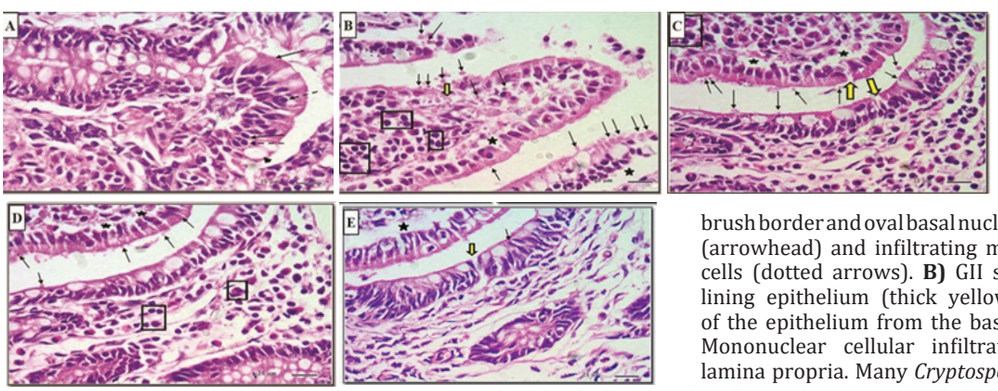

Fig. 1. H&E-stained sections of ileal tissue explant (H&E x1000). **A)** GI showing normal epithelial lining composed of columnar enterocytes (thin arrows) with intact brush border and oval basal nuclei, in addition to goblet cells (arrowhead) and infiltrating mononuclear inflammatory cells (dotted arrows). **B)** GII showing disruption of the lining epithelium (thick yellow arrow) and separation of the epithelium from the basement membrane (stars). Mononuclear cellular infiltration (rectangles) in the lamina propria. Many *Cryptosporidium* in different stages of development (thin arrows) are also seen scattered on the ileal mucosal surface and at sites of epithelial disruption. **C)** GIII showing many different-sized parasitic stages (thin arrows) on the mucosal surface. Disruption of the lining epithelium (thick yellow arrows) and its separation from the basement membrane (stars), as well as mononuclear cellular infiltration of the lamina propria, can be seen. **D)** GIV showing few oocysts (thin arrows) on the epithelial surface with their focal separation from the basement membrane (stars). Notice mononuclear cellular infiltration (rectangles) in the lamina propria. **E)** GV showing normal lining epithelium (thin arrow). Focal disruption (thick arrow) and focal separation of the lining epithelium (star) can be noticed.

Table 1. Semiquantitative assessment of histopathological changes in the different studied groups.

Histopatholoical changes	Groups				Statistical analysis	
	G II	G III	G IV	G V	X^2	*P*
Inflammatory cell infiltrate						
Minimal	0	0	2	5		
Mild	0	1	2	1	39.358	**0.001***
Moderate	1	1	1	0		
Severe	5	4	1	0		
Interruption of the lining epithelium						
Minimal	0	0	2	5		
Mild	0	1	3	1	42.988	**0.001***
Moderate	2	2	1	0		
Severe	4	3	0	0		
Separation of the lining cells from the underlying basement membrane						
Minimal	0	0	2	6		
Mild	0	1	3	0	55.512	**0.001***
Moderate	1	2	1	0		
Severe	5	3	0	0		

N.B. Data represent the number of ileal explants in each group. X^2: Chi-square; ***:** Significant ($P<0.05$).

III (NTZ-treated infected explants) showed minimal improvement. Some parasitic stages of different sizes and shapes and having irregular, rough surfaces, were observed on the ileal mucosal surface. The enterocytes had eroded or flattened irregular surfaces with lost intercellular demarcations. Interruption of the mucosal surface was also observed in some sections (Fig. 2D). Group V (AUR-treated infected explants) showed more improvement of the previously detected changes in G II. Few shrunken, irregularly-shaped parasitic stages were occasionally detected in a few sections. In addition, loss of demarcation, flattening, and irregularity of the surface of some enterocytes were still observed (Fig. 2E). Group V (combined NTZ and AUR treatment) showed marked improvement of the histopathological changes previously detected in G II, with restoration of normal architecture of the ileal mucosal surface, villi, and enterocytes. However, lost demarcation was occasionally observed between a few enterocytes with no parasitic stages observed (Fig. 2F).

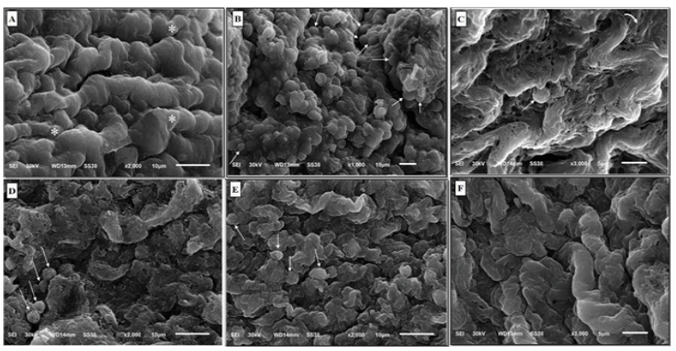

Fig. 2. Scanning electron micrograph of the ileal tissue explants. **A)** GI showing normal brush border with the normal architecture of the ileal mucosal surface. The enterocytes **(*)** appeared polygonal with a dome-shaped upper surface (SEM ×2000). **B)** GII showing a disrupted ileal mucosal surface with multiple scattered different-sized parasitic stages with regular shape and smooth surface (thin arrows) (SEM ×1000). **C)** GII showing eroded, irregular intestinal surface and lost intercellular demarcations with exposure of underlying connective tissue (curved arrow) and one parasitic stage (thin arrow) (SEM ×3000). **D)** GIII showing enterocytes with eroded, irregular rough surface and lost intercellular demarcations, and some parasitic stages with an irregular rough surface (thin arrows) (SEM ×2000). **E)** G IV showing intact intestinal surface with little disruption, and some shrunken parasitic stages with irregular rough surface (thin arrows) (SEM ×2000). **F)** GV showing marked improvement with no *C. parvum* oocysts. (SEM ×3000).

Transmission electron microscopic study: Group I (negative uninfected explant group) showed normal ultrastructure of the ileal lining epithelium that was formed of enterocytes and goblet cells. The enterocytes were tall columnar cells joined by intercellular junctions (tight junction, zonula adherens, and desmosomes). They displayed regularly arranged, closely packed apical microvilli and oval basal euchromatic nuclei. The cytoplasm contained numerous mitochondria and rough endoplasmic reticulum (RER). Goblet cells containing mucin-secreting granules were also detected (Fig. 3A). Group II (positive infected explant group) showed a remarkable loss of the normal ultrastructure of the ileal lining cells. Many enterocytes revealed rarefied or vacuolated cytoplasm, damaged or swollen mitochondria, and dilated RER. Some enterocytes revealed loss of the microvilli and/or disruption of the apical cell membrane. Shrunken dense nuclei were detected in a few cells (Fig. 3B, 3C). In addition, *C. parvum* parasites were detected at different developmental stages (Fig. 4). Group III (NTZ-treated infected explants) showed some improvement of the ultrastructural changes detected in the ileal lining cells of G II. Many enterocytes and goblet cells appeared more or less normal; however, some enterocytes displayed cytoplasmic vacuoles, dilated RER, and apical displacement and/or flattening of the nuclei (Fig. 3D). Group IV (AUR-treated infected explants) showed marked improvement of the ultrastructure of the lining cells. However, some enterocytes still show apical

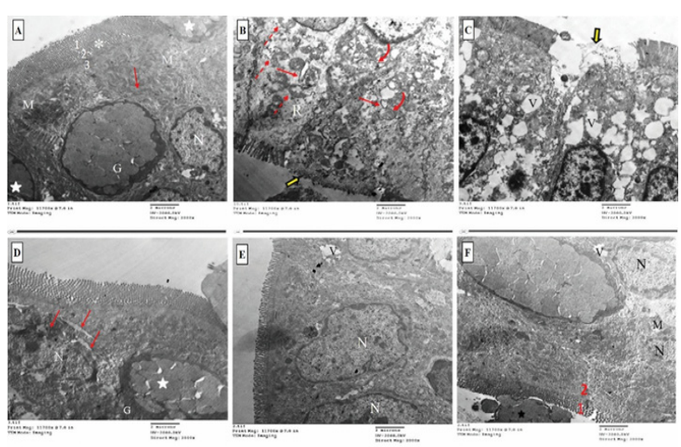

Fig. 3. Transmission electron micrograph of ileal tissue explant (TEM ×2000). A) GI showing normal enterocytes that appear as tall columnar cells joined by intercellular junctions (1 tight junction, 2 zonula adherens, and 3 desmosomes) with closely packed apical microvilli (*) and oval basal euchromatic nucleus (N). Abundant mitochondria (M) and RER (thin red arrow) are seen in the cytoplasm and normal mucin-secreting granules (stars) of the goblet cells (G). B) GII showing enterocytes with rarefied cytoplasm (R), damaged (dashed arrows) or swollen mitochondria (curved arrows), dilated RER (thin arrows), and loss of the apical microvilli (thick yellow arrow). C) GII showing enterocytes with multiple large cytoplasmic vacuoles (V), disruption of the apical cell membrane, and loss of the microvilli (thick yellow arrow). D) GIII showing enterocytes with RER dilatation (thin red arrows), apical displacement, flattening of the enterocyte nucleus (N), and mucin granules (star) of a goblet cell (G). E) GIV showing enterocytes with apical nuclear displacement (N) and few cytoplasmic vacuoles (V). F) GV showing normal enterocytes joined together by intercellular junctions (1 tight junction and 2 zonula adherens), intact, closely packed microvilli (*), rounded to oval nuclei (N), RER (thin red arrows), mitochondria (M), a few small cytoplasmic vacuoles (V) and numerous normal mucin-secreting granules (stars) of the goblet cells.

nuclear displacement, few cytoplasmic vacuoles, and few swollen mitochondria (Fig. 3E). Group V (combined NTZ and AUR treatment) showed remarkable improvement of the ileal lining cells' ultrastructure. The enterocytes had continuous intact microvilli and apparent tall columnar with rounded to oval basal euchromatic nuclei, mitochondria, and RER. The cells were joined together by intercellular junctions (tight junction and zonula adherens); only occasional small cytoplasmic vacuoles were noted (Fig. 3F).

Biochemical results: As shown in table (2), levels of IFN-γ and IL-1β showed significant elevation (P<0.05) in the infected control group as compared to the normal control group. Additionally, there was a significant (P<0.001) decrease in their mean levels in all treated groups as compared to the infected control group. The lowest levels were reported in the combined treated group, with no significant difference compared to the normal control group. Levels of IL-10 showed a significant (P<0.001) decrease in the infected control group (190.57±18.67) as compared to the normal control group (863.23±67.37). Its level in all treated groups was significantly higher than that of the infected control group. The combined treated group showed the highest level of IL-10 (768.52±34.74) (Table 2). Regarding TrxR activity, the mean level in the infected control group

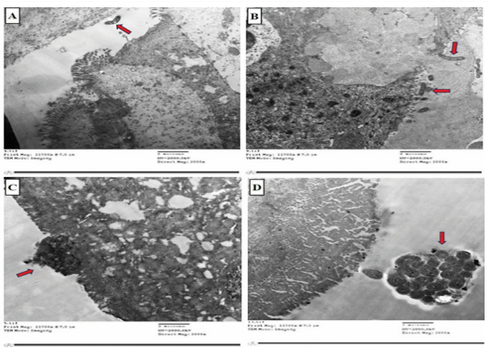

Fig. 4. Different developmental stages of *C. parvum* (red arrows) as seen in diverse transmission electron micrographs of the ileum of G II; **A, B**: Merozoites. **C:** Trophozoite, **D:** Meront.

(19.92±2.64) was significantly (P=0.001) lower than that of the negative control group (33.59±1.00). Its level in the NTZ group (22.80±2.36) was not significantly different from that in the infected control group. The combined treated group (17.02±1.11) showed no significant difference compared to the infected control group. There was also a significant (P=0.002) decrease in its level in the AUR group (14.31±0.72) as compared to the infected control group. There was no significant difference between AUR and the combined treated groups, but the AUR group had the lowest TrxR level.

Table 2. Levels of cytokines and TrxR in the study groups.

Groups	IFN-γ Mean ± SD	Statistical analysis				
		KWχ^2	*P*1	*P*2	*P*3	*P*4
G I	79.47 ± 4.30					
G II	362.43 ± 15.98		**<0.001***			
G III	230.56 ± 10.95	23.077	**<0.001***	**<0.001***		
G IV	189.15 ± 16.41		**<0.001***	**<0.001***	**<0.001***	
G V	99.57 ± 3.37		= 0.155	**<0.001***	**<0.001***	**<0.001***
	IL-1β Mean ± SD	**Statistical analysis**				
		KWχ^2	*P*1	*P*2	*P*3	*P*4
G I	114.11 ± 8.27					
G II	411.12 ± 23.35		**<0.001***			
G III	286.45 ± 12.75	22.907	**<0.001***	**<0.001***		
G IV	201.22 ± 13.47		**<0.001***	**<0.001***	**<0.001***	
G V	135.18 ± 6.54		= 0.274	**<0.001***	**<0.001***	**<0.001***
	IL-10 Mean ± SD	**Statistical analysis**				
		KWχ^2	*P*1	*P*2	*P*3	*P*4
G I	863.23 ± 67.37					
G II	190.57 ± 18.67		**<0.001***			
G III	313.46 ± 32.38	22.737	**<0.001***	**<0.001***		
G IV	493.76 ± 27.16		**<0.001***	**<0.001***	**<0.001***	
G V	768.52 ± 34.74		**= 0.024***	**<0.001***	**<0.001***	**<0.001***
	TrxR Mean ± SD	**Statistical analysis**				
		KWχ^2	*P*1	*P*2	*P*3	*P*4
G I	33.59 ± 1.00					
G II	19.92 ± 2.64		**<0.001***			
G III	22.80 ± 2.36	21.415	**<0.001***	= 0.190		
G IV	14.31 ± 0.72		**<0.001***	**<0.002***	**<0.001***	
G V	17.02 ± 1.11		**<0.001***	= 0.185	**<0.001***	= 0.238

KWX^2: Chi-square for Kruskal-Wallis test; ***P*1:** Comparison with GI; ***P*2:** Comparison with GII; ***P*3:** Comparison with GIII; ***P*4:** Comparison with GIV; ***:** Significant (P<0.05).

DISCUSSION

Cryptosporidium spp. are apicomplexan protozoa with a worldwide distribution[26]. It is an important cause of diarrhea that is responsible for thousands of infant and toddler deaths annually. Moreover, infection may be complicated by long-term deficits in growth and cognitive functions[27]. Nitazoxanide is the only FDA-approved medication for the treatment of cryptosporidiosis. However, it has a limited efficacy, especially in immunocompromised patients, even at high doses[28]. Thus, there is an urgent need for the development of a more effective anti-cryptosporidial agent.

Auranofin is a FDA-approved drug for rheumatoid arthritis. It demonstrated effectiveness against various viral, bacterial, and parasitic infections[8]. The TrxR enzyme has been identified as a potential drug target due to its crucial role in the metabolic processes and survival of the parasite within the host. Of note, AUR exerts its anti-protozoal effects primarily through inhibition of the antioxidant enzyme TrxR, thereby inducing oxidative stress and the production of reactive oxygen species (ROS), leading to intrinsic apoptosis of parasites[29]. Accordingly, the present study aimed to evaluate the efficacy of AUR in comparison with NTZ and their combination on *C. parvum* infection in an *ex vivo* study.

In our study, the ileal mucosa of the infected, untreated group exhibited significant alterations, including interruption of the lining epithelium with separation of the lining cells from the underlying basement membrane, and many endogenous developmental stages of *C. parvum* clinging to the brush border of the villi. These findings agreed with those of Aboelsoued *et al.*[20] who detected numerous parasitic stages attached to the surface of the *C. parvum*-infected, untreated ileal tissue explants. The mechanical effect of the parasite stages on the intestinal mucosa was considered the cause of the damaging morphological changes. These results were consistent with those of other studies[30,31]. However, Yahia *et al.*[32] capitulated that toxins released by *Cryptosporidium* could cause direct harm to the epithelial cells. Furthermore, it was conceded that cryptosporidiosis in mice may cause epithelial dysplastic alterations and stratification[33].

The previous changes were also reported in the NTZ-treated group, where multiple parasitic stages of different sizes were seen spreading along the ileal surface, causing disruption of the epithelial lining. The assumption of NTZ inefficiency against *C. parvum in vitro* was documented by Shalaby *et al.*[30] who denoted the higher efficacy of romidepsin over NTZ in reducing oocyst reproductivity. Whitta *et al.*[34] also denoted a higher efficacy and safety of the pyrazolopyridine analogue KDU731 over NTZ *in vitro*.

In the present study, the pathological changes were mild and less observed in the AUR group, accompanied by a few scattered oocysts spreading on the ileal surface. In agreement with our results, several studies reported the efficacy of AUR in killing other parasites. An *in vitro* assay of *Schistosoma* showed that AUR rapidly killed juvenile and adult forms of *S. mansoni*[14]. Additionally, Rady *et al.*[35] found that AUR significantly decreased *F. gigantica* adult motility and egg hatching. Similarly, AUR exhibited inhibitory effects against the promastigote stage of *L. tropica*[12]. Furthermore, an *in vitro* assay demonstrated that *E. histolytica* trophozoites treated with AUR became increasingly susceptible to oxidative stress in a time-dependent manner. Besides its activity against the trophozoites, AUR also appears to exert an effect on the cysts of *E. invadens*, the only ameba known to readily encyst *in vitro*[6]. Moreover, *G. lamblia* assemblages A and B were found to be susceptible to AUR, as demonstrated by Argüello-García *et al.*[29] who reported that AUR could overcome resistance to metronidazole.

The SEM examination revealed that the most severe pathological changes occurred in the infected, untreated group, where different parasitic stages were scattered along the irregular, disturbed intestinal surface, showing multiple defects that may be attributed to *C. parvum* release from the infected intestinal tissue. These findings are confirmatory to our histopathological analysis. In the same context, Vélez *et al.*[19] reported similar changes in bovine small intestinal explants with multiple intracellular parasitic stages detected from 3-24 h PI. We also noted parasite-driven hole-like lesions in the affected intestinal villi surface. This too was in agreement with another report[36] that studied the development of *C. parvum* in human ileocecal adenocarcinoma (HCT-8) cell culture and observed the parasitic stages with the hole-like defects on the surface of host cells, which were suggested to be induced by the parasite release. The NTZ-treated group showed mild improvement in the pathological features of the disease, while the AUR-treated group showed marked improvement with regression and severe deformity of parasitic stages. Minimal pathology was observed in the group treated with combined NTZ-AUR therapy, with nearly no parasites detected.

In the ultrastructural evaluation by TEM, the infected untreated group showed a remarkable loss of the normal ultrastructure of the ileal lining cells. The most striking finding in our results was the significant abnormality in the shape and disruption of the mitochondria. Mitochondria play a crucial role in cellular homeostasis and innate immunity by their balanced response to intracellular or extracellular stimuli[37]. Infections, including cryptosporidiosis, disrupt mitochondrial homeostasis, thereby impairing its ability to generate the energy required for cellular survival[38].

In the present study, ultrastructural examination revealed that the NTZ-treated group exhibited only

mild improvement in the ileal epithelial architecture. In contrast, the AUR-treated group showed marked restoration of the ultrastructure, while the combined NTZ-AUR treatment group demonstrated the most notable improvement, with the ileal lining cells closely resembling those of the uninfected control group.

Our findings confirm the research of Esmat *et al.*[1]. The observed dilatation of the RER in the infected groups in our study may be a consequence of either liquid buildup due to the osmotic imbalance or a failure of the synthetic function. Besides, the intestinal mucosa of the infected, untreated explants also displayed signs of rarefaction and cytoplasmic vacuolation. This damage could explain how the infection with *C. parvum* impacts enterocyte permeability, ion transfer, and water and sodium chloride absorption, leading to diarrhea. Our present study also reported evidence of mitochondrial degradation and swelling, which agrees with McKay *et al.*[38] who described how *Cryptosporidium*-induced mitochondrial degeneration diminishes this vital organelle's capability to produce the energy essential for regular cellular regeneration, causing cellular toxicity and death.

Regarding the inflammatory markers assay, IFN-γ displayed a significant role in the immune response against cryptosporidiosis, both in early innate immune and cell-mediated responses. Consequently, it interferes with the invasion and growth of parasites by direct action on the enterocytes. Moreover, the proinflammatory cytokine IL-1β induces inflammation by acting on immune cells such as neutrophils and macrophages, as well as non-immune cells, as smooth muscle and vascular endothelial cells. Furthermore, a chief defensive factor in the intestine is IL-10, a regulatory anti-inflammatory cytokine. It is regarded as a key modulator of intestinal homeostasis and immunological responses in the gastrointestinal tract. It inhibits mucosal inflammatory and immunological responses and is produced by a wide range of intestinal mucosal cells. Thus, it may arrest the excessive reactions of the immune system that threaten the host during the infection[39].

In our present research, the infected untreated group showed a significant increase in IFN-γ and IL-1β levels as compared to the normal control group. Conversely, there was a significant decrease in their mean levels in all treated groups compared to the infected untreated group. The lowest level was observed in the NTZ-AUR combined group. On the other hand, the level of IL-10 in the infected untreated group was significantly lower than that of the normal control group, and its level in all treated groups was significantly higher than that in the infected untreated group. Among all treated groups, the NTZ-AUR combined group showed the highest level of IL-10. These findings were in accordance with other studies[20,40]. In agreement with our results, Nasralla *et al.*[41] observed a reduction in IL-10 levels during cryptosporidiosis. They concluded that this cytokine was not involved in the development of the disease in cryptosporidiosis. Thus, it may be a main factor in the repair of the intestinal epithelium during cryptosporidiosis.

Additionally, in agreement with our results, recent research suggests that NTZ can combat the cytokine storm in cryptosporidiosis via suppressing the production of pro-inflammatory cytokines[42]. Similarly, Al-Kuraishy *et al.*[43] demonstrated that NTZ can diminish the inflammatory reactions accompanying acute respiratory syndrome coronavirus 2 (SARS-CoV-2) through inhibiting the production of pro-inflammatory cytokines. Concerning the NTZ-AUR combined therapy, it apparently exerted the best results with a significant reduction in IFN-γ and IL-1β levels and a significant increase in IL-10 levels, nearly attaining their recorded levels in the normal control group. This result suggests the synergistic effect of NTZ and AUR that can lead to a greater overall effect.

Studies on schistosomiasis *mansoni*[14], and amoebiasis[22] confirmed the dual anti-parasitic and anti-inflammatory effects of AUR. Pasche *et al.*[14] reported AUR efficacy in killing adult worms of *S. mansoni in vitro*. Moreover, AUR induced a significant decrease in the worm count in mice infected with *S. mansoni*[44]. Additionally, AUR's anti-inflammatory action via blocking inflammasome activation helped in reducing liver granuloma and fibrosis induced by *S. mansoni*[45].

As regards the antioxidant TrxR enzyme, we found that its mean level in the infected untreated group was significantly lower than that of the normal control group. However, in the AUR group, there was a highly significant decrease in its mean level when compared to the infected untreated group. This agreed with Argüello-García *et al.*[29] who concluded that AUR exerted an *in vitro* anti-giardial effect by targeting the TrxR enzyme. The inhibition of redox enzymes such as TrxR is considered the chief mechanism of action of AUR. Inhibition of TrxR enzyme modifies the redox state of the cell, stimulating the release of hydrogen peroxide and reactive oxygen species (ROS), leading to intrinsic apoptosis of cells[15].

The oxidant effect of AUR was proved by several studies. For example, Abou-El-Naga *et al.*[46] demonstrated that the AUR-treated group achieved a significant elevation in the *T. gondii*-induced (ROS) levels. Moreover, Chmelyuk *et al.*[15] found that AUR induced anticancer effects on glioblastoma by stimulating ROS production and decreasing TrxR enzyme. In our study, the combined treated group fell between the NTZ and AUR groups due to the different effects of both drugs on the TrxR enzyme.

In conclusion, the present study described the potential therapeutic effect of AUR in cryptosporidiosis and its synergistic effect when combined with NTZ. AUR approved its efficacy as a novel anti-cryptosporidial

drug in an *ex vivo* study. It was superior to NTZ as an anti-parasitic and anti-inflammatory agent. Marked improvement of the intestinal histopathological and ultrastructural changes was obtained by AUR and NTZ-AUR combined therapy, but the highest effect was achieved in the combined treated group, with restoration of the normal intestinal architecture. The combination of AUR and NTZ showed better results than monotherapy with either of them. Therefore, AUR can be considered as an effective adjuvant that potentiates the action of NTZ and overcomes its resistance problems. Additionally, further *in vivo* and human studies should focus on the mechanism of action of AUR against *C. parvum* and investigate different doses and/or durations of AUR that can obtain the best effects on cryptosporidiosis.

Author contribution: El-saadi EG contributed to the study design, practical work, statistical analysis, and writing the original draft. Deyab FA contributed to the study design and critical revision for the final approval. Ismail HIH contributed to the study design and critical revision for the final approval. Sadek MT contributed to the practical work, statistical analysis, and critical revision for the final approval. Elkaliny HH contributed to the practical work. Elgendy DI contributed to the study design, practical work, statistical analysis, writing the original draft, and critical revision for the final approval. All authors accepted the final version of the manuscript before publication.

Conflicts of interest: There is no conflict of interest.

Funding statement: None.

REFERENCES

1. Esmat M, Abdel-Aal AA, Shalaby MA, Badawi M, Elaskary H, Yousif AB, *et al.* Efficacy of clofazimine and nitazoxanide combination in treating intestinal cryptosporidiosis and enhancing intestinal cellular regeneration in immunocompromised mice. Food Waterborne Parasitol 2022; 27:e00161.
2. Guo F, Zhang H, McNair NN, Mead JR, Zhu G. The existing drug vorinostat as a new lead against cryptosporidiosis by targeting the parasite histone deacetylases. J Infect Dis 2018; 217(7):1110-1117.
3. Bouzid M, Kintz E, Hunter PR. Risk factors for *Cryptosporidium* infection in low- and middle-income countries: A systematic review and meta-analysis. PLoS Negl Trop Dis 2018; 12(6): e0006553.
4. Checkley W, White AC Jr, Jaganath D, Arrowood MJ, Chalmers RM, Chen XM, *et al.* A review of the global burden, novel diagnostics, therapeutics, and vaccine targets for *Cryptosporidium*. Lancet Infect Dis 2015; 15(1):85-94.
5. Vinayak S. Recent advances in genetic manipulation of *Cryptosporidium*. Curr Opin Microbiol 2020; 58:146-152.
6. Andrade RM, Reed SL. New drug target in protozoan parasites: The role of thioredoxin reductase. Front Microbiol 2015; 6:975.
7. Cui XY, Park SH, Park WH. Anti-cancer effects of auranofin in human lung cancer cells by increasing intracellular ROS levels and depleting GSH levels. Molecules 2022; 27(16):5207.
8. Feng L, Pomel S, Latre de Late P, Taravaud A, Loiseau P M, Maes L, *et al.* Repurposing auranofin and evaluation of a new gold(i) compound for the search of treatment of human and cattle parasitic diseases: From protozoa to helminth infections. Molecules 2020; 25(21):5075.
9. Hopper M, Yun JF, Zhou B, Le C, Kehoe K, Le R, *et al.* Auranofin inactivates *Trichomonas vaginalis* thioredoxin reductase and is effective against trichomonads *in vitro* and *in vivo*. Int J Antimicrob Agents 2016; 48(6):690-694.
10. Yason JA, Koh KARP, Tan KSW. Viability screen of LOPAC1280 reveals phosphorylation inhibitor auranofin as a potent inhibitor of *Blastocystis* subtype 1, 4, and 7 isolates. Antimicrob Agents Chemother 2018; 62(8):e00208-18.
11. Escrig JI, Hahn HJ, Debnath A. Activity of auranofin against multiple genotypes of *Naegleria fowleri* and its synergistic effect with amphotericin B *in vitro*. ACS Chem Neurosci 2020; 11(16):2464-2471.
12. Yıldırım A, Özbilgin A, Yereli K. Antiprotozoal activity of auranofin on *Trypanosoma cruzi, Leishmania tropica* and *Toxoplasma gondii*: *in vitro* and *ex vivo* study. Trans R Soc Trop Med Hyg 2023; 117(10):733-740.
13. Bulman CA, Bidlow CM, Lustigman S, Cho-Ngwa F, Williams D, Rascón AA Jr, *et al.* Repurposing auranofin as a lead candidate for treatment of lymphatic filariasis and onchocerciasis. PLoS Negl Trop Dis 2015; 9(2):e0003534.
14. Pasche V, Laleu B, Keiser J. Early anti-schistosomal leads identified from *in vitro* and *in vivo* screening of the medicines for malaria venture pathogen box. ACS Infect Dis 2019; 5(1):102-110.
15. Chmelyuk N, Kordyukova M, Sorokina M, Sinyavskiy S, Meshcheryakova V, Belousov V, *et al.* Inhibition of thioredoxin-reductase by auranofin as a pro-oxidant anticancer strategy for glioblastoma: *in vitro* and *in vivo* studies. Int J Mol Sci 2025; 26(5):2084.
16. Abhishek S, Sivadas S, Satish M, Deeksha W, Rajakumara E. Dynamic basis for auranofin drug recognition by thiol-reductases of human pathogens and intermediate coordinated adduct formation with catalytic cysteine residues. ACS Omega 2019; 4(5):9593-9602.
17. Lee SM, Koh DH, Jun DW, Roh YJ, Kang HT, Oh JH, *et al.* Auranofin attenuates hepatic steatosis and fibrosis in nonalcoholic fatty liver disease via NRF2 and NF-κB signaling pathways. Clin Mol Hepatol 2022; 28(4):827-840.
18. Ch Stratakos A, Sima F, Ward P, Linton M, Kelly C, Pinkerton L, *et al.* The *in vitro* and *ex vivo* effect of Auranta 3001 in preventing *Cryptosporidium hominis* and *Cryptosporidium parvum* infection. Gut Pathog 2017; 9:49.
19. Vélez J, Silva LMR, Gärtner U, Daugschies A, Mazurek S, Hermosilla C, *et al.* First metabolic insights into *ex vivo Cryptosporidium parvum*-infected bovine small intestinal explants studied under physioxic conditions. Biology (Basel) 2021; 10(10):963.
20. Aboelsoued D, Toaleb NI, Abdel Megeed KN, Hassan SE, Ibrahim S. Cellular immune response and scanning electron microscopy in the evaluation of *Moringa* leaves aqueous extract effect on *Cryptosporidium parvum* in buffalo intestinal tissue explants. J Parasit Dis 2019; 43(3):393-401.

21. Mahgoub AMA, Gameil MA, Abdelgawad M, Wanas H, Hamed AMR. *In vitro* molecular assessment of *Cryptosporidium parvum* parasitic load on human ileocecal adenocarcinoma cell culture after targeting by tavaborole (AN2690). J Parasit Dis 2025; 49(1):84-92.
22. Mi-Ichi F, Ishikawa T, Tam VK, Deloer S, Hamano S, Hamada T, *et al.* Characterization of *Entamoeba histolytica* adenosine 5'-phosphosulfate (APS) kinase; validation as a target and provision of leads for the development of new drugs against amoebiasis. PLoS Negl Trop Dis 2019; 13(8):e0007633.
23. Atallah MA, El-Kowrany SI, Afifi OK, Elkaliny HH, Younis SS, Gamea GA. *In vivo* study on the anti-parasitic effect of omeprazole on *Cryptosporidium parvum* in Mice. Parasite Immunol 2025; 47(6):e70012.
24. Wang L, Liu D, Gao Y, Hou Z, Zhu Y, Wang F, *et al.* Examination of gametocyte protein 22 localization and oocyst wall formation in *Eimeria necatrix* using laser confocal microscopy and scanning electron microscopy. Parasit Vectors 2023; 16(1):124.
25. Duranova H, Valkova V, Knazicka Z, Olexikova L, Vasicek J. Mitochondria: A worthwhile object for ultrastructural qualitative characterization and quantification of cells at physiological and pathophysiological states using conventional transmission electron microscopy. Acta Histochem 2020; 122(8):151646.
26. Abbas Z, Khan MK, Abbas RZ, Sindhu ZUD, Sajid MS, Munir A, *et al.* Molecular Epidemiology of *Cryptosporidium parvum* and *Giardia lamblia* in different water bodies, soil, and vegetables in Pakistan. Health Secur 2022; 20(4):308-320.
27. Kotloff KL, Nasrin D, Blackwelder WC, Wu Y, Farag T, Panchalingham S, *et al.* The incidence, etiology, and adverse clinical consequences of less severe diarrheal episodes among infants and children residing in low-income and middle-income countries: A 12-month case-control study as a follow-on to the global enteric multicenter study (GEMS). Lancet Glob Health 2019; 7(5):e568-e584.
28. Widmer G, Carmena D, Kváč M, Chalmers RM, Kissinger JC, Xiao L, *et al.* Update on *Cryptosporidium* spp.: Highlights from the seventh international *Giardia* and *Cryptosporidium* conference. Parasite 2020; 27:14.
29. Argüello-García R, Leitsch D, Skinner-Adams T, Ortega-Pierres MG. Drug resistance in *Giardia*: mechanisms and alternative treatments for giardiasis. Adv Parasitol 2020; 107:201-282.
30. Shalaby NE, Shoheib ZS, Yassin NA, El-Kaliny HH, Hasby Saad MA. Pyroptosis tuning in intestinal cryptosporidiosis *via* the natural histone deacetylase inhibitor romidepsin. Parasite Immunol 2024; 46(3):e13032.
31. Moneer EA, Akl SH, Shahin YH, Elwakil BH, Eskandrani A, Paudel KR, *et al.* The antiparasitic effect of C-Phycocyanin nanoparticles on cryptosporidiosis in immunosuppressed mice. J Parasit Dis 2025; 49(1):173-185.
32. Yahia SH, El Gamal RL, Fathy GM, Al-Ghandour AMF, El-Akabawy N, Abdel-Hameed BH, *et al.* The potential therapeutic effect of *Nigella sativa* and *Zingiber officinale* extracts versus nitazoxanide drug against experimentally induced cryptosporidiosis in laboratory mice. J Parasit Dis 2023; 47(2):329-339.
33. Abdelhamed EF, Fawzy EM, Ahmed SM, Zalat RS, Rashed HE. Effect of nitazoxanide, artesunate loaded polymeric nano fiber and their combination on experimental cryptosporidiosis. Iran J Parasitol 2019; 14(2):240-249.
34. Whitta STG, Lamont B, Suwanarusk R, Russell BM, Muhsin-Sharafaldine MR. Comparative efficacy and safety of anti-cryptosporidial agents: An *in vitro* study on nitazoxanide, halofuginone lactate, KDU731, and paromomycin against *Cryptosporidium parvum*. Front Microbiol 2024; 15:1463457.
35. Rady AA, Nassef NE, El-Shafey OK, Beshay EV, Mahmoud SF, Abougalalah DI, *et al. In vitro* evaluation of thioredoxin reductase inhibitor (Auranofin) activity in comparison with triclabendazole on adult *Fasciola gigantica*. J Egypt Soc Parasitol 2021; 51(1):213-226.
36. Vélez J, Velasquez Z, Silva LMR, Gärtner U, Failing K, Daugschies A, *et al.* Metabolic signatures of *Cryptosporidium parvum*-infected HCT-8 cells and impact of selected metabolic inhibitors on *C. parvum* infection under physioxia and hyperoxia. Biology (Basel) 2021; 10(1):60.
37. Han B, Lin CJ, Hu G, Wang MC. 'Inside out'- a dialogue between mitochondria and bacteria. FEBS J 2019; 286(4):630-641.
38. McKay DM, Mancini NL, Shearer J, Shutt T. Perturbed mitochondrial dynamics, an emerging aspect of epithelial-microbe interactions. Am J Physiol Gastrointest Liver Physiol 2020; 318(4):G748-G762.
39. Papoutsopoulou S, Pollock L, Walker C, Tench W, Samad SS, Bergey F, *et al.* Impact of interleukin 10 deficiency on intestinal epithelium responses to inflammatory signals. Front Immunol 2021; 12:690817.
40. de Sablet T, Potiron L, Marquis M, Bussière FI, Lacroix-Lamandé S, Laurent F. *Cryptosporidium parvum* increases intestinal permeability through interaction with epithelial cells and IL-1β and TNFα released by inflammatory monocytes. Cell Microbiol 2016; 18(12):1871-1880.
41. Nasralla BA, Mohammed NS, Muhsen SS. Gene sequences of TNF and INFα cytokines in *Cryptosporidium* co-infection with *H. pylori* of irritable bowel syndrome. J Biosci Appl Res 2024; 10(2):129-39.
42. Lu W, Yang F, Meng Y, An J, Hu B, Jian S, *et al.* Immunotoxicity and transcriptome analysis of zebrafish embryos exposure to nitazoxanide. Fish Shellfish Immunol 2023; 141:108977.
43. Al-Kuraishy HM, Al-Gareeb AI, Elekhnawy E, Batiha GE. Nitazoxanide and COVID-19: A review. Mol Biol Rep 2022; 49(11):11169-11176.
44. Kim HY, Kim KS, Kim MJ, Kim HS, Lee KY, Kang KW. Auranofin inhibits RANKL-induced osteoclastogenesis by suppressing inhibitors of κB kinase and inflammasome-mediated interleukin-1β Secretion. Oxid Med Cell Longev 2019; 2019:3503912.
45. Atia AF, Abou-Hussien NM, Sweed DM, Sweed E, Abo-Khalil NA. Auranofin attenuates *Schistosoma mansoni* egg-induced liver granuloma and fibrosis in mice. J Helminthol 2023; 97:e95.
46. Abou-El-Naga IF, Mogahed NMFH. Repurposing auranofin for treatment of experimental cerebral toxoplasmosis. Acta Parasitol 2021;66(3):827-836.